An evaluation of seismic modeling with the lowrank method

Schleicher, J.*, Costa, J. C.†, Novais, A.*, Landeta B., A. V.* (*: UNICAMP & INCT-GP, †: UFPA & INCT-GP)

Abstract

The numerical simulation of wave propagation can be represented by a propagator matrix applied to previous instances of the wavefield. To make this procedure feasible, the propagator matrix must be approximated by a low-rank representation. While the underlying idea is to correctly represent the kinematics of the wavefield with no particular regard to its dynamics, it is important to understand its amplitude properties. Therefore, in this work, we evaluate the absolute and relative performance of the lowrank method for the simulation of 2D acoustic wave propagation with respect to its dynamic quality. We start our analysis in homogeneous media, where theoretical expressions for the wavefield are available. We find that the method provides not only an excellent kinematic approximation, but also reliable amplitudes. In our implementation, the quality of the dynamics was affected by the temporal sampling interval. Choosing a model-dependent time sampling, we could confine the dynamic error to less than 1% for all tested models. Next we tested the quality of the simulated reflection coefficients in media with a single horizontal reflector in comparison with the theoretical results and those obtained using a standard second-order finite-difference (FD) method (implementation from SU). The reflection coefficients approximated by the lowrank method were of the same quality or slightly superior to those obtained by FD. It is to be stressed that, while comparing unfavorably with FD regarding computation time for small models, its quasi-linear scaling with model size makes the lowrank method superior for large models.

Introduction

Over the years, the reflection seismic method has been applied in order to obtain accurate subsurface information. For this, it is crucial to understand and being able to simulate seismic waves propagation, e.g. in applications like reverse-time migration or full-waveform inversion. In this context, various methods for numerical modeling of seismic waves have been proposed.

Since the analytical solution of the wave equation is only possible in very simple media, numerical approximations are needed to approximate the wavefields in real media. One of the most used methods is the extrapolation in time, approximating the partial derivatives by a finite-difference (FD) scheme (Etgen, 1986). Another way often employed is the use of spectral methods that apply the Fourier transform to the wave equation to manipulate it in the domains of the variables associated with the spectrum, that is, the temporal frequency and the spatial frequency or wavenumber, associated with the coordinates of time and space, respectively. A relatively recent method is the modeling of wave propagation by the *lowrank* method. It comprises the approximation of the wave propagation operator in the mixed domain of space and wavenumber. The *lowrank* decomposition makes use of the sparsity of the propagator matrix, selecting a lower-dimensional set of representative spatial locations and a lower-dimensional set of representative wavenumbers (Fomel et al., 2013). In this work, we evaluate this latter method to numerically approximate wave propagation in 2D acoustic media. Although the method is derived based on kinematic arguments, we are particularly interested in evaluating its dynamic behavior.

Wave Equation Extrapolation

The 3D acoustic wave equation with constant density is given by

$$\frac{\partial^2}{\partial t^2} P(\mathbf{x},t) = v^2 \Delta P(\mathbf{x},t), \tag{1}$$

where v denotes the propagation velocity, and P is the acoustic wavefield. Considering the constant velocity, one can apply the spatial Fourier transform, defined in this paper by

$$\hat{P}(\mathbf{k},t) = \frac{1}{(2\pi)^3} \int_{-\infty}^{\infty} P(\mathbf{x},t) e^{-i\mathbf{x}\cdot\mathbf{k}} d\mathbf{x}, \tag{2}$$

By the inverse Fourier transform, given a fixed initial t_0, the acoustic pressure for $t = t_0 + \Delta t$ can be represented by

$$P(\mathbf{x},t_0+\Delta t) = \int_{-\infty}^{\infty} \hat{P}(\mathbf{k},t_0) e^{i[\mathbf{x}\cdot\mathbf{k} - v\|\mathbf{k}\|\Delta t]} d\mathbf{k}. \tag{3}$$

To generalize the last procedure to a medium with a varying velocity, one can use the candidate

$$P(\mathbf{x},t_0+\Delta t) = \int_{-\infty}^{\infty} \hat{P}(\mathbf{k},t_0) e^{i\phi(\mathbf{x},\mathbf{k},\Delta t)} d\mathbf{k}, \tag{4}$$

where $\phi(\mathbf{x},\mathbf{k},\Delta t)$ represents a generalized phase function defined in the mixed domain of space and wave number. Substituting the derivatives of the candidate into the wave equation, we obtain two differential equations for ϕ,

$$\left(\frac{\partial \phi}{\partial t}\right)^2 = v^2 |\nabla \phi|^2, \tag{5}$$

e

$$\frac{\partial^2 \phi}{\partial t^2} = v^2 \Delta \phi, \tag{6}$$

which can be satisfied simultaneously.

Extracting the square root of the first expression, we find that ϕ must satisfy

$$\frac{\partial \phi}{\partial t} = \pm v|\nabla \phi|, \tag{7}$$

where we choose the positive sign, which is associated with the outward propagation direction.

We now consider the Taylor series of the phase operator around $\Delta t = 0$

$$\phi(\mathbf{x},\mathbf{k},\Delta t) = \phi_0(\mathbf{x},\mathbf{k}) + \phi_1(\mathbf{x},\mathbf{k})\Delta t + \phi_2(\mathbf{x},\mathbf{k})\frac{\Delta t^2}{2} + O(\Delta t^3), \tag{8}$$

where $\phi_n = \left.\frac{\partial^n \phi}{\partial t^n}\right|_{\Delta t=0}$. The initial condition of the phase function is obtained when substituting $\Delta t = 0$ in equation (4). In this case, the equation must reduce to the inverse Fourier transform, which implies

$$\phi_0(\mathbf{x},\mathbf{k}) = \phi(\mathbf{x},\mathbf{k},0) = \mathbf{x}\cdot\mathbf{k}. \tag{9}$$

It follows that ϕ can be written as

$$\phi(\mathbf{x},\mathbf{k},\Delta t) = \mathbf{x}\cdot\mathbf{k} + \phi_1(\mathbf{x},\mathbf{k})\Delta t + \phi_2(\mathbf{x},\mathbf{k})\frac{\Delta t^2}{2} + O(\Delta t^3). \tag{10}$$

The terms ϕ_1 and ϕ_2 represent the first and second time derivatives of ϕ and can be approximated by imposing equations (6) and (7).

By calculating the gradient with respect to $\mathbf{x}$ of the last expression it is possible to obtain a linear approximation for the gradient of the phase function ϕ, given by

$$|\nabla\phi| \approx \|\mathbf{k}\| + \frac{\nabla\phi_1\cdot\mathbf{k}}{\|\mathbf{k}\|}\Delta t. \tag{11}$$

On the other hand, by deriving the Taylor series with respect to time and neglecting second order terms

$$\frac{\partial\phi}{\partial t} \approx \phi_1(\mathbf{x},\mathbf{k}) + \phi_2(\mathbf{x},\mathbf{k})\Delta t. \tag{12}$$

The use of approximations (11) and (12) in (7) and equating the terms of equal powers of Δt results in

$$\phi_1(\mathbf{x},\mathbf{k}) = v\|\mathbf{k}\|, \tag{13}$$

and

$$\phi_2(\mathbf{x},\mathbf{k}) = v(\nabla v\cdot\mathbf{k}). \tag{14}$$

Substituting these last two expressions into the equation (10), we can conclude that

$$\phi(\mathbf{x},\mathbf{k},\Delta t) \approx \mathbf{x}\cdot\mathbf{k} + v(\mathbf{x})\|\mathbf{k}\|\Delta t + v(\mathbf{x})(\nabla v\cdot\mathbf{k})\frac{\Delta t^2}{2}. \tag{15}$$

We are looking for an approximation for the phase function $\phi(\mathbf{x},\mathbf{k},\Delta t)$ for small steps Δt. Therefore, in equation (15) we can neglect the second-order terms onwards, which leads to the following expression for the phase function

$$\phi(\mathbf{x},\mathbf{k},\Delta t) \approx \mathbf{x}\cdot\mathbf{k} + v(\mathbf{x})\|\mathbf{k}\|\Delta t. \tag{16}$$

The last equation was previously derived by Etgen & Brandsberg-Dahl (2009). The form of the phase function in equation (16) is particulary attractive because it immediately allows to generalize the approximation (4). It remains applicable when one has a closed expression for the phase velocity in the mixed space $(\mathbf{x},\mathbf{k})$, i.e., $v = v(\mathbf{x},\mathbf{k})$. Then, equation (4) becomes

$$P(\mathbf{x},t_0+\Delta t) \approx \int_{-\infty}^{\infty} \hat{P}(\mathbf{k},t_0) e^{i[\mathbf{x}\cdot\mathbf{k} + v(\mathbf{x})\|\mathbf{k}\|\Delta t]} d\mathbf{k}. \tag{17}$$

While equation (17) could be directly applied for wave propagation, it can be modified to avoid a complex propagator matrix. Using this equation again to express $P(\mathbf{x},t_0-\Delta t)$, adding the two together and subtracting $2P(\mathbf{x},t_0)$, we can write

$$\begin{aligned} P(\mathbf{x},t_0+\Delta t) &\approx 2P(\mathbf{x},t_0) - P(\mathbf{x},t_0-\Delta t) \\ &\quad + 2\int \hat{P}(\mathbf{k},t_0) e^{i\mathbf{x}\cdot\mathbf{k}} [\cos(v(\mathbf{x})\|\mathbf{k}\|\Delta t) - 1] d\mathbf{k}. \end{aligned} \tag{18}$$

Our implementation makes use of this form, which relies on a real-valued propagator matrix and helps to stabilize the numerical computations.

As we can see from equation (4), the basic idea of this wave-propagation procedure is based on kinematic considerations, superimposing wavefields in a kinematically correct way in order to predict the wavefield at a later time. However, being an approximate generalization of equation (3), which is an exact solution of the acoustic wave equation for constant v, we can expect an approximately correct dynamic behavior. It is for this reason that we performed our numerical experiments to evaluate the dynamics of this approximation.

Wave extrapolation matrix

By discretizing the equation (18), we can write it as

$$P_{j,s+1} = 2P_{j,s} - P_{j,s-1} + \sum_l \Delta\mathbf{k} W_{jl} \hat{P}_{l,s} e^{i\mathbf{x}_j\cdot\mathbf{k}_l} \tag{19}$$

where $P_{j,n} = P(\mathbf{x}_j,t_n)$, $\hat{P}_{l,n} = P(\mathbf{k}_l,t_n)$, and W_{jl} denotes the wave extrapolation matrix, defined by

$$W_{jl} = W(\mathbf{x}_j,\mathbf{k}_l) \approx 2[\cos(v(\mathbf{x}_j,\mathbf{k}_l)\|\mathbf{k}_l\|\Delta t) - 1]. \tag{20}$$

Matrix $\mathbf{W}$ has dimension $N_x \times N_k$, where N_x and N_k are the dimensions of the vectors $\mathbf{x}$ and $\mathbf{k}$, respectively, the dimensions of the full model and wavenumber spaces, because $\mathbf{W}$ depends on the spatial and spectral variables. Thus $\mathbf{W}$ is a large but sparse matrix. The goal of the *lowrank* method is to take advantage of the sparsity and decompose the matrix using smaller dimension matrices. That is, an approximate factorization of (20) is sought, with fixed Δt, of the form

$$W(\mathbf{x},\mathbf{k}) \approx \sum_{m=1}^{M_k}\sum_{n=1}^{M_x} U(\mathbf{x},\mathbf{k}_m) M_{mn} V(\mathbf{x}_n,\mathbf{k}), \tag{21}$$

where M_x and M_k are significantly smaller dimensions than N_x and N_k. Substituting (21) into (19), we obtain

$$P_{j,s+1} = 2P_{j,s} - P_{j,s-1} + \sum_{m=1}^{M_k} U_{jm}\left[\sum_{n=1}^{M_x} M_{mn}\sum_l \Delta\mathbf{k} V_{nl}\hat{P}_{l,s} e^{i\mathbf{x}_j\cdot\mathbf{k}_l}\right], \tag{22}$$

where the innermost sum is the discrete Fourier transform of $V_{n,l}\hat{P}_{l,s}$. Because of the significantly lower dimensions of the inner matrix M_{mn}, the number of floating point operations in equation (22) is greatly reduced.

Lowrank decomposition

Here, we describe the procedure to find an adequate representation of the inner matrix M_{mn} and the transformation matrices U_{jm} e V_{nl}.

The idea of the *lowrank* method is to find a lowrank approximation of a sparse matrix **W** of rank r, defined by the factorization

$$\mathbf{W} \approx \mathbf{UMV}^*, \tag{23}$$

where $*$ denotes the adjoint matrix, i.e., the conjugate of the transposed matrix. Here, **U** is a submatrix that consists of a set Π_1 of columns associated with $\{\mathbf{k}\}$ approximating $\mathbf{W}(:,\Pi_1)$, $\mathbf{V}^*$ is a submatrix that consists in the subsest Π_2 of rows associated with $\{\mathbf{x}\}$ approximating $\mathbf{W}(\Pi_2,:)$ and **M** is a $r \times r$ matrix with complete rank equal to r.

The submatrices **U** and $\mathbf{V}^*$, both orthonormal, are constructed such that the columns of **U** and the rows of $\mathbf{V}^*$ can accurately generate the column space and the row space of **W**, respectively. The algorithm starts by selecting a random set Ω_1 of a sufficiently large number of columns of **W**. Generally, 3 or 4 times the expected rank r of **W** is sufficient. To obtain the largest possible r-dimensional parallelepiped, we compute the QR-decomposition with column pivoting (Meyer, 2000) of $\mathbf{W}(:,\Omega_1)$. In our numerical experiments, the resulting rank r was estimated by the following stopping criterion: If the ratio between the first and the current pivot of the QR factorization is smaller than 10^{-6}, the decomposition is stopped and the rank r is equal to the number of pivots in the previous step. Thus, we have $\mathbf{Q}_1$ from

$$\mathbf{W}(:,\Omega_1)\mathbf{P}_1 = \mathbf{Q}_1\mathbf{R}_1, \tag{24}$$

where $\mathbf{P}_1$ is the column permutation matrix, $\mathbf{Q}_1$ is the orthogonal matrix and $\mathbf{R}_1$ is the upper triangular matrix. Then, the first r pivot columns of $\mathbf{Q}_1$ will form the set Π_1 of columns in U. In practice it is observed that the volume of the parallelepiped generated by the columns in $\mathbf{U}(:,\Pi_1)$ is always close to the maximum possible volume. This is a consequence of the oscillatory nature of the columns in **W** (Fomel et al., 2013).

Analogously to the previous step, one chooses a similar-sized set Ω_2 of rows of **W** and searches for the r-dimensional parallelepiped with largest volume. For this, one computes the QR decomposition with column pivoting on $\mathbf{W}(\Omega_2,:)^*$, to obtain

$$\mathbf{W}(\Omega_2,:)^*\mathbf{P}_2 = \mathbf{Q}_2\mathbf{R}_2. \tag{25}$$

It follows that the first r pivot rows of the matrix $\mathbf{Q}_2$ will form the Π_2 set of rows in $\mathbf{V}^*$.

Once the matrices **U** and **V** are computed, the next step is to obtain the low rank matrix $\mathbf{M} : r \times r$ such that $\mathbf{W} \approx \mathbf{UMV}^*$. To reduce the cost of determining the matrix **M**, Fomel et al. (2013) propose to choose a set Y of s random rows and a set Z of s random columns of **W** and minimize

$$\min_{\mathbf{M}} \|\mathbf{W}(Y,Z) - \mathbf{U}(Y,:)\mathbf{MV}^*(Z,:)\|_F. \tag{26}$$

The result of the minimization procedure (26) can be explicitly represented as

$$M = (U(Y,:))^\dagger \cdot W(Y,Z) \cdot (V^*(:,Z))^\dagger, \tag{27}$$

where $(\cdot)^\dagger$ indicates the pseudo-inverse.

Results

Homogeneous medium

In a homogeneous medium, the analytical solution of the wave equation is given by the convolution between the source function and the Green's function. This allow to evaluate the accuracy of the numerical solution, obtained by the *lowrank* method.

Our first model called model A (901×451), is a 2D homogeneous medium with propagation velocity 2000 m/s, a surface extension of 9 km and a depth of 4.5 km, discretized with a spatial sampling interval Δx = Δz = 10 m. For the first numerical experiment, we used an injector source located at 4.5 km from the origin with a depth of 1 km. The maximum propagation time was 2 s with a time sampling interval Δt = 0.001 s. The receiver is located at 4.5km from the source at a depth of 3 km. The pulse injected into the impulsive source is a Ricker wavelet with a peak frequency of 5 Hz. To obtain the reference analytical response as a variation of the wavefield as a function of time, we compute the convolution of the pulse and the 2D Green's function.

Figure 1 shows the temporal traces of the analytical solution and that obtained using the *lowrank* method, which show an excellent coincidence. The pulse shape in the two traces is almost identical, with *lowrank* slightly overestimating the amplitude. The arrival time of the events is indistinguishable and their value of 1 s is correct for the propagation distance of 2 km in a medium with a velocity of 2000 m/s. The relative dynamic error of the modeling considering the peak of the traces was 0.015 %. The numerically estimated rank r of the propagator matrix was equal to 2.

To verify wether the slight differences of the pulses in the traces in Figure 1 are the consequence of a kinematic error or a phase error of the modeled pulse, we have calculated

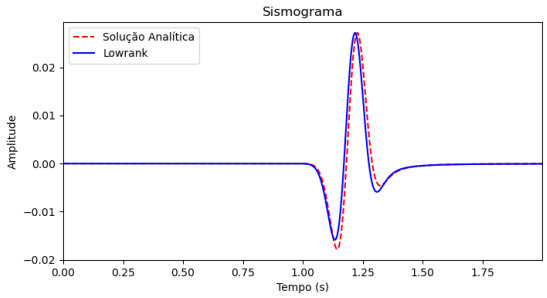

Figura 1 – Comparison of the temporal traces of the analytical solution with the solution obtained using the lowrank method on model A with Δt = 0.001 s.

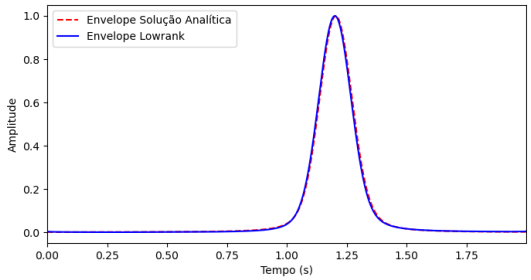

Figura 2 – Temporal envelopes of the analytical solution with the solution obtained using the lowrank method on model A with Δt = 0.001 s.

the normalized envelopes of the analytical solution and the approximation obtained using the lowrank method, shown in Figure 2. Since the envelopes are virtually identical, we conclude that the travel time of the pulses is correct, and the fact that the pulses in Figure 1 are not fully coincident is due to a phase difference between the pulses.

From this experiment, we conclude that the lowrank method is capable of calculating highly accurate numerical approximations to acoustic wave propagation in a homogeneous medium.

To check wether the quality is comparable with that of the finite difference method, we compared our results to those obtained with the **sufdmod2** program of Seismic Un*x. The latter program uses the traditional second-order approximation in time and space for the partial derivatives in the wave equation. Since this program fixes the time sampling interval automatically so that the stability of the method is obeyed, we used the same Δt for the *lowrank* method in this comparison.

For this experiment with model A, the SU program fixes the temporal sampling interval at 0.0025 s. Figure 3 shows the snapshot of the propagation at time t = 1.5 s, modeled by the *lowrank* method (Figure 3a) and by finite differences (Figure 3b). We observe two very similar results, the only perceptible difference being the different shape of the border reflection at the top, caused by a different quality of the absorbing boundaries.

The amplitude scaling of the modeled wavefield is different, though, as revealed by the comparison of the vertical traces at the source position in these snapshots (compare the lowrank result in Figure

We note that the direct wave is kinematically positioned correctly in both slices, but that the amplitudes are dfferent by an order of magnitude. We can also observe the different format and positioning of the boundary reflection. Note that for this example, the FD result is free of the noticeable numerical dispersion. Other spatial discretizations led to perceptible dispersion.

Considering again the receiver located at 4.5 km from the origin and at a depth of 3 km, the temporal traces of the modelings are compared correspondingly with respect to the analytical solution. Figure 6 shows the temporal traces of the analytical, *lowrank* and finite difference solutions. To be able to plot the traces approximated by the two methods in a single figure, we have normalized them by an amplitude scale, determined by the peak amplitude ratio between the analytical solution and the approximate traces. The resulting scale factor for the *lowrank* method was 1.02 and for finite differences, 0.06. Note that for the given discretization, the *lowrank* method slightly undersizes the wave, while, finite differences considerably oversizes the theoretical solution. By comparison with the previous experiment, in which only the time sampling was different, we note a small amplitude decay with increasing sampling rate of the lowrank method. This behavior has been confirmed by means of other experiments not shown here.

Analysis of the Reflection Coefficients

To analyse whether the lowrank method can also well approximate the amplitudes of reflected waves, we devised another experiment with a single planar horizontal reflector. In such a model, the reflection coefficients should be well approximated by the theoretical formulas for the plane wave reflection coefficients.

Our specific model B has again a horizontal extension of 9 km and a depth of 4.5 km with a spatial sampling of 10 m. It consists of a homogeneous overburden with a wave speed of 2000 m/s and a single planar horizontal reflector at a depth of 2 km. The velocity of the medium below the reflector was 2200 m/s.

To determine the reflection coefficients obtained by the *lowrank* and finite difference methods without any perturbation by the direct wave and boundary effects, we performed three numerical experiments. The source is located at the same position for all three experiments, being at x = 4500 m, z = 1000 m. For the first experiment we recorded the wave propagating in model B with an arrangement of 200 receivers at the depth of 500 m, spaced 10 m apart with a *end-on spread* configuration and one receiver at normal incidence. The second and third experiments consider a homogeneous medium with the same dimensions as model B and a constant wave velocity of the upper part of model B, i.e., 2000 m/s. In the second experiment, we record the wavefield in this model at the same receivers of the first experiment, and in the third experiment, we record it at the mirror receivers, positioned symmetrically to the original receivers with respect to the reflector position. In this way, the propagation distance, and thus the traveltime and geometrical spreading, to the mirror receivers in the third experiment are the same as for the reflected wave in the first experiment. Thus, by subtracting the result of the second experiment, which contains only the direct wave and possible boundary reflections, from the result of the first experiment, we extract the reflected event. Dividing this difference by the result of the third experiment, we obtain the approximate reflection coefficients as simulated by the respective method.

In this experiments, we fixed the temporal sampling interval for *lowrank* at 0.001 s, while the one for finite differences was determined by the program using the stability condition. For model B, the temporal discretization of finite differences was 0.00227273 s, which was then

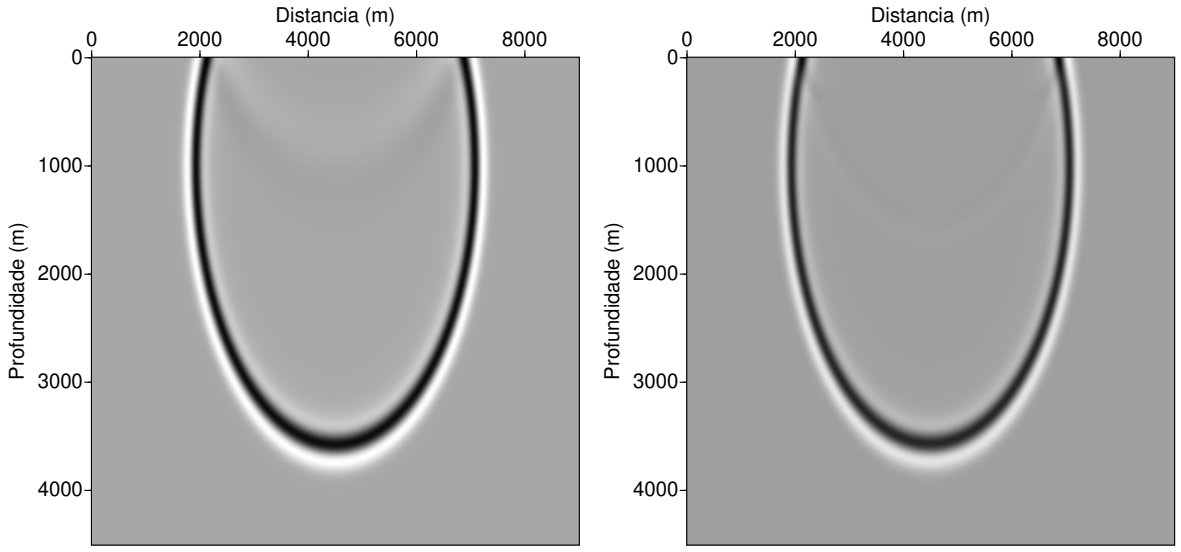

(a) *Lowrank* Approximation (b) Finite Differences

Figura 3 – Wavefield snapshot in model A with an wave source located 4.5 km from the source with a depth of 1000 m after 1.5 s.

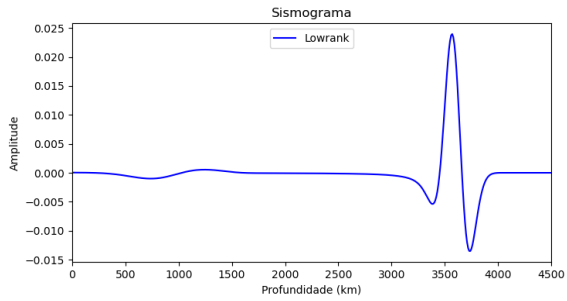

Figura 4 – Vertical spatial slice through the lowrank wavefield snapshots at the source position in Figure 3(a).

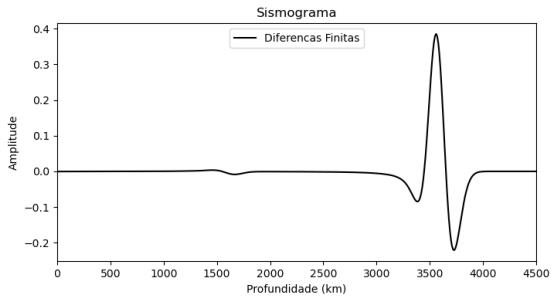

Figura 5 – Vertcial spatial slice through the FD wavefield snapshots at the source position in Figure 3(b).

fixed for all three numerical computations. Figure 7 shows the reflected event recorded at normal incidence after subtracting the direct wave (blue line) and the direct wave at the corresponding mirror receiver (green line) as modeled by the lowrank method. As expected, the events are kinematically coincident. The ratio of these traces defines the modeled reflection coefficient at normal incidence.

Correspondingly, the reflection coefficients at other incidence angles are given by the ratios between the reflected wave recorded at the original receivers in model B and the wave recorded at the mirror receivers in the homogeneous medium. Figure 8 shows the approximations of the reflection coefficients for model B, obtained from lowrank (solid blue line) and FD (solid green line), as compared to the theoretical reflection coefficients (dashed red line)

We notice a very good approximation of the reflection coefficients by the *lowrank* and finite differences methods. Actually, comparing the relative errors of the achieved approximations, shown in Figure 9, we can see that the approximation by the lowrank method (blue line) is even somewhat better than the one by FD (black line). Overall, the relative errors of lowrank are lower and show less fluctuation than those of the finite differences method. Other experiments with other velocity contrasts at the reflector confirm our findings reported here. Generally, the lowrank reflection coefficients are slightly better than the FD reflection coefficients.

Discussion and Conclusions

By means of numerical experiments in different models, we have evaluated the absolute and relative performance of 2D acoustic modeling using the *lowrank* method, particularly with regard to the quality of the resulting amplitudes. For the first part of the experiments, we considered homogeneous media, in order to compare the numerical results to the analytical solution of the

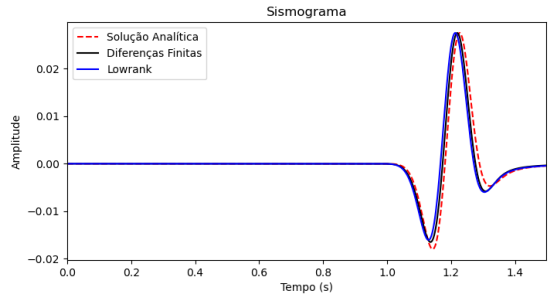

Figura 6 – Comparison of the temporal traces of the analytical solution with the solution obtained using the lowrank method and finite differences on model A with Δt = 0.0025 s.

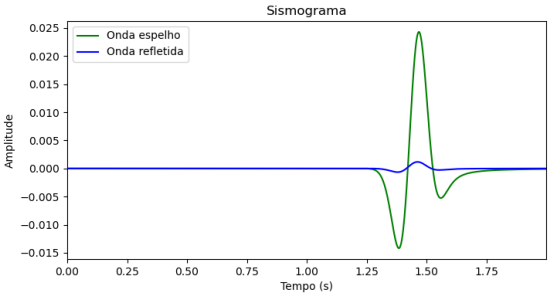

Figura 7 – Experiments illustration performed to approximate the reflection coefficients.

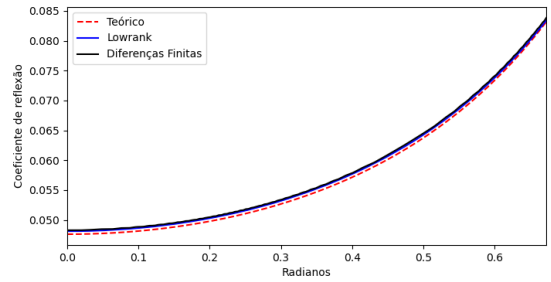

Figura 8 – Comparison of theoretical reflection coefficients with lowrank method and finite differences for model B.

wave equation. In this way, we studied the response of the lowrank method for various discretizations of the same model, and compared it to the theoretical response in kinematics and dynamics. From our tests, we conclude that the quality of the results depend on the spatial and temporal discretization, but it for every spatial discretization, it was always possible to find a temporal sampling interval for which the *lowrank* method presents a dynamic error smaller than 1%. The reference numerical solution, obtained by the finite difference code from Seismic Un*x, produced less reliable amplitudes. Moreover, it is more sensitive to numerical dispersion for coarse spatial discretizations. This also affects the kinematics as the waves tend to arrive slightly earlier than

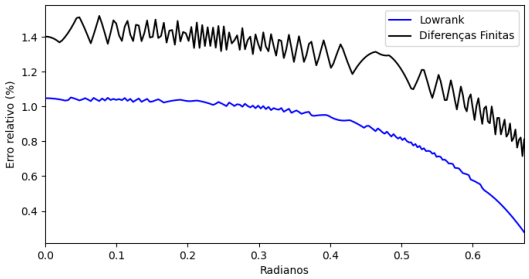

Figura 9 – Relative error of the reflection coefficients approximated by the lowrank method and finite differences for model B.

the theoretical solution. It is to be observed that there is no dispersion effect in lowrank modeling.

In a second set of tests, we evaluated the reflection coefficients modeled by the lowrank method, again in comparison to the SU FD code. Even though the *lowrank* method does not explicitly include any amplitude effects, the acoustic reflection coefficients are well approximated.

Summarizing, our tests have demonstrated that the lowrank method can produce reliable acoustic wavefields, both regarding traveltimes and amplitudes. This is particularly important for large-scale problems, because the computing cost of lowrank modeling scales much more favorably with model size than that of Finite Differences. Future studies will have to be carried out so as to evaluate wether this excellent amplitude behaviour can also be achieved in more general media, particulary those exhibiting anisotropy.

Acknowledgements

The authors are grateful for the support of our working groups by Petrobras as well as the Brazilian agencies CNPq (supporting the INCT-GP) and CAPES (student scholarship).

References

Etgen, J. T., 1986. High-order finite-difference reverse time migration with the 2-way non-reflecting wave equation.

Etgen, J. T. & Brandsberg-Dahl, S., 2009. The pseudo-analytical method: Application of pseudo-Laplacians to acoustic and acoustic anisotropic wave propagation, SEG Technical Program Expanded Abstracts, vol. 28(1): 2552–2556, doi:10.1190/1.3255375.

Fomel, S., Ying, L. & Song, X., 2013. Seismic wave extrapolation using lowrank symbol approximation, Geophysical Prospecting, vol. 61(3): 526–536, doi: 10.1111/j.1365-2478.2012.01064.x.

Meyer, C. D., 2000. Matrix Analysis and Applied Linear Algebra, SIAM.